



HAL
open science

Y-shaped magnonic demultiplexer using induced transparency resonances

Abdelkader Mouadili, El Houssaine El Boudouti, Abdellatif Akjouj, Housni Al-Wahsh, Bahram Djafari-Rouhani, L. Dobrzynski

► **To cite this version:**

Abdelkader Mouadili, El Houssaine El Boudouti, Abdellatif Akjouj, Housni Al-Wahsh, Bahram Djafari-Rouhani, et al.. Y-shaped magnonic demultiplexer using induced transparency resonances. *AIP Advances*, 2019, 9 (3), pp.035011. 10.1063/1.5080350 . hal-03143601

HAL Id: hal-03143601

<https://hal.science/hal-03143601>

Submitted on 24 May 2022

HAL is a multi-disciplinary open access archive for the deposit and dissemination of scientific research documents, whether they are published or not. The documents may come from teaching and research institutions in France or abroad, or from public or private research centers.

L'archive ouverte pluridisciplinaire **HAL**, est destinée au dépôt et à la diffusion de documents scientifiques de niveau recherche, publiés ou non, émanant des établissements d'enseignement et de recherche français ou étrangers, des laboratoires publics ou privés.



Distributed under a Creative Commons Attribution 4.0 International License

Y-shaped magnonic demultiplexer using induced transparency resonances

Cite as: AIP Advances 9, 035011 (2019); <https://doi.org/10.1063/1.5080350>

Submitted: 07 November 2018 • Accepted: 25 February 2019 • Published Online: 11 March 2019

 A. Mouadili,  E. H. El Boudouti,  A. Akjouj, et al.



View Online



Export Citation



CrossMark

ARTICLES YOU MAY BE INTERESTED IN

[Experimental and theoretical evidence for the existence of photonic bandgaps and selective transmissions in serial loop structures](#)

Journal of Applied Physics **95**, 1102 (2004); <https://doi.org/10.1063/1.1633983>

[The design and verification of MuMax3](#)

AIP Advances **4**, 107133 (2014); <https://doi.org/10.1063/1.4899186>

[Acoustical multi-frequency filtering by a defective asymmetric phononic serial loop structure](#)

AIP Advances **10**, 075313 (2020); <https://doi.org/10.1063/5.0011208>



Read Now!

AIP Advances
Biophysics & Bioengineering Collection

Y-shaped magnonic demultiplexer using induced transparency resonances

Cite as: AIP Advances 9, 035011 (2019); doi: 10.1063/1.5080350

Submitted: 7 November 2018 • Accepted: 25 February 2019 •

Published Online: 11 March 2019



View Online



Export Citation



CrossMark

A. Mouadili,¹  E. H. El Boudouti,^{2,a)}  A. Akjouj,³  H. Al-Wahsh,⁴ B. Djafari-Rouhani,³ and L. Dobrzynski³ 

AFFILIATIONS

¹Laboratoire de Physique de la Matière Condensée et Énergie Renouvelable, Département de Physique, Faculté des Sciences et Techniques de Mohammedia, Université Hassan II, 20650 Casablanca, Morocco

²Laboratoire de Physique de la Matière et du Rayonnement, Département de Physique, Faculté des Sciences, Université Mohammed I, 60000 Oujda, Morocco

³Institut d'Électronique, de Microélectronique et de Nanotechnologie (IEMN), UMR CNRS 8520, Département de Physique, Université Lille, 59655 Villeneuve d'Ascq, France

⁴Engineering Mathematics and Physics Department, Faculty of Engineering, Benha University, 11629 Cairo, Egypt

^{a)}Corresponding author: elboudouti@yahoo.fr

ABSTRACT

We give an analytical demonstration of the possibility to realize a simple magnonic demultiplexer based on induced transparency resonances. The demultiplexer consists on an Y-shaped waveguide with an input line and two output lines. Each line contains two grafted stubs at a given position far from the input line. We derive in closed form the analytical expressions for selective transfer of a single propagating mode through one line keeping the other line unaffected. This is performed through magnonic induced transparency resonances (MIT) characterized by a resonance squeezed between two transmission zeros. The existence of a complete transmission beside a zero transmission, enables to select a given frequency on one output line, by canceling the transmission on the second line as well as the reflection in the input line. Also, we show that despite the existence of a bifurcation of the input line on two output lines, the transmission through each line can be written following a Fano line shape. In addition, in order to understand better the scattering properties of the filtered resonances, we give the analytical expressions of Fano parameter q and quality factor Q of the MIT resonance in each line. The spatial distribution of the spin waves associated to different MIT resonances is performed through an analysis of the magnetization of these modes. Also, the effect of attenuation on the transmission spectra and the quality of demultiplexing is also discussed. The theoretical results are performed using the Green's function approach which enables to deduce in closed form, the transmission and reflection coefficients as well as the densities of states.

© 2019 Author(s). All article content, except where otherwise noted, is licensed under a Creative Commons Attribution (CC BY) license (<http://creativecommons.org/licenses/by/4.0/>). <https://doi.org/10.1063/1.5080350>

I. INTRODUCTION

The rapid development of research on magnonic crystals (MCs) is related to the possibility of using spin waves as a new means of signal processing, communication and computation over a very wide bandwidth. The developments in the field of spin dynamics, such as the interaction of charge and heat currents with magnons, opens up the prospect of new concepts of information processing and potential applications purely magnetic without the need of charge transport.^{1,2} Magnons are the spin-wave excitation quanta of magnetic materials. They can be classically understood as the collective precession of electron spins.^{1,3-11}

The magnonic devices may be smaller than conventional microwave devices because the spin waves operating at GHz or THz frequencies have micron or nanometric wavelength and the information can be encoded in either the amplitude^{7,12} or in the phase¹³ of the spin waves. Interest in MCs also results from their potential use as high sensitive magnetic sensors,¹⁴ switches,^{15,16} couplers,¹⁷⁻¹⁹ tunable filters or phase shifters,²⁰⁻²² multiplexers⁷ and transistors.²³

The existence of the analogue of electromagnetic induced transparency (EIT) and Fano resonances in classical linear systems such as phononic, photonic and plasmonic structures, has attracted a great deal of attention.²⁴⁻²⁷ In this context, we have shown

theoretically and experimentally the possibility of existence of these two types of resonances^{28,29} in simple photonic circuits composed of a waveguide with two grafted stubs on the same site or at two different sites. These resonances are obtained by detuning the lengths of the two stubs of lengths d_1 and d_2 (i.e., $\delta = d_2 - d_1$). The coupling of spin waveguides with one or more resonators has been studied and applied to obtain the so-called *magnonic induced transparency* (MIT) resonances.³⁰⁻³² This process can also be applied to the design of a wavelength magnonic crystal demultiplexer.

In a recent paper,³⁰ we have shown the possibility of existence of the induced transparency resonances in a simple magnonic circuit made of a waveguide with two grafted stubs at the same site. Such resonances are obtained by detuning the lengths of the two stubs of lengths d_1 and d_2 (i.e., $\delta = d_2 - d_1$) in such a way that the two stubs induce two transmission zeros falling at two closed frequencies f_1 and f_2 . Then there exists automatically a third frequency f_3 lying between f_1 and f_2 for which the transmission reaches unity. This resonance, squeezed between two transmission zeros, has been shown to be induced by the two stubs taken together. In this work, we show the possibility to realize a simple magnetic demultiplexer based on such induced resonances.³⁰ The demultiplexer consists of an Y-shaped waveguide with an input line and two output lines (Fig. 1). Each line contains two grafted stubs at a given position far from the input line. The existence of transmission zeros around the MIT resonances enables us to derive in closed form the expressions for selective transfer of a single propagating mode through one line keeping the other line unaffected. We illustrate these analytical results by some numerical solutions for a simple structure made out of one-dimensional magnetic waveguides. In addition, the exact results are supported by approximate results (Taylor expansion) around the resonances showing that the transmission coefficients can be written following a Fano like form where the position, width and Fano parameters of the resonances can be deduced explicitly as a function of δ . The theoretical results are obtained using the Green's function method which enables to deduce in closed form the transmission and reflection coefficients as well as the densities of states.

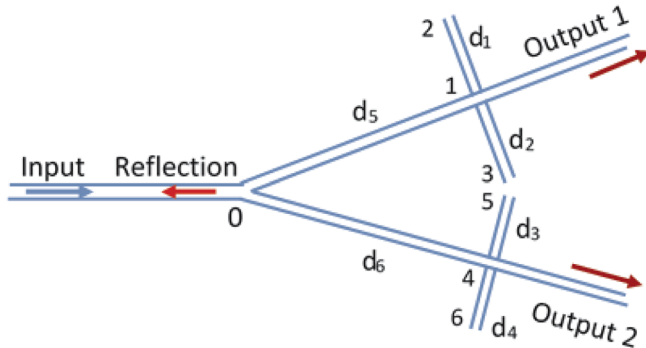


FIG. 1. Schematic representation of a demultiplexer in the Y-shape with one input line and two output lines. Along the first output line, two stubs of lengths d_1 and d_2 are inserted at the same position on the waveguide and at a distance d_5 from the input line. Along the second output line, two stubs of lengths d_3 and d_4 are inserted at the same position on the waveguide at a distance d_6 from the input line.

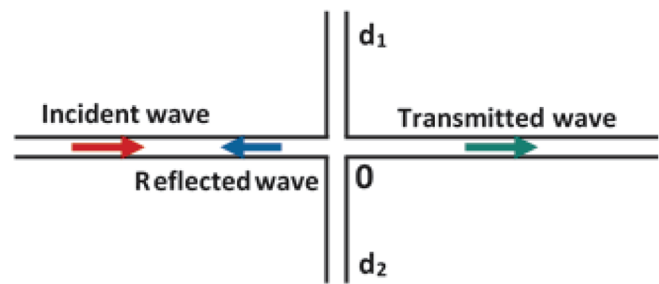


FIG. 2. Schematic illustration of the one dimensional waveguide with two resonators on the same site. The lengths of the resonators are d_1 and d_2 .

This paper is organized as follows: in section II, we give a summary of the method of calculation and the possibility to obtain the induced transparency resonances in a cross structure (Fig. 2). Section III is devoted to the calculation of transmission and reflection coefficients based on the Green's function method. In this section we present also the analytical results that enable to achieve a complete transmission in one line by canceling the transmission in the second line as well as the reflection in the input line. In addition we give some numerical results to elucidate the obtained phenomenon. The spatial localization of the different modes transferred and stopped along each line are analyzed by means of the magnetization field. Also, the effect of damping on the transmission spectra in each line is discussed. In section IV, we summarize and conclude the main results of this work.

II. MIT RESONANCE IN DETUNED MAGNONIC STUB WAVEGUIDES: AN OVERVIEW

It is well established^{33,34} that properties of spin waves are mainly determined by two important interactions acting between magnetic moments: the magnetic dipole and the exchange interaction. Since the contribution of the exchange interaction is scaled with wavevector as k^2 (see Eq. (1) below), for relatively small wavevectors ($k < 10^4 \text{ cm}^{-1}$) the spin wave dynamics is almost entirely determined by the magnetic dipole interaction and magnetostatic modes are the resulting excitations that propagate in such waveguides.³⁵ Due to the anisotropic nature of the magnetic dipole interaction, the frequency of a spin wave depends not only on the absolute value of its wavevector, but also on the orientation of the wavevector relative to the static magnetization. However, for large values of wavevectors ($k > 10^6 \text{ cm}^{-1}$), the exchange interaction, which thus provides the restoring force for spin waves, dominates although there is also interest in the intermediate (or dipole-exchange) case, where both types of interactions influence the dynamical behavior. This is a first step towards more sophisticated calculations, in particular on the effects of longer-ranged interactions, which are expected to produce some changes in the position and shape of the MIT resonance whose existence is mainly reported here. In this work, we use the classical ferromagnetic Heisenberg model where the Hamiltonian is constituted only by the part that presents the exchange interaction. Therefore, in evaluating the needed Green's function, it is convenient to use the continuum approximation. This approximation is valid provided that the wavelengths are large compared to

the lattice spacing and to the transverse dimension of the waveguide. In this case the propagation becomes monomode.³⁶ In our case even if the wavelength is small ($1/k < 10^{-6} \text{cm}$), it is still considered higher than the transversal section of the waveguide in order to consider monomode propagation along with Heisenberg approximation. Also, the magnetization and the applied magnetic field are supposed to be perpendicular to the plane of Fig. 1 (i.e. the deviation from the static magnetization are in the direction of the waveguides).

In this long wavelength exchange interaction model, the dispersion relation of the magnons can be written as

$$\omega = \gamma H_0 + Dk^2, \quad (1)$$

where $D = (2Ja^2 M_0)/(\gamma \hbar^2)$. ω , M_0 , H_0 , J , γ and \hbar stand respectively for the angular frequency of the spin wave, the spontaneous magnetization, the static external field, the exchange interaction between neighboring magnetic sites in the lattice of lattice parameter a constituting the ferromagnetic medium, the gyromagnetic ratio and the Planck constant.³⁶ The calculation of transmission and reflection coefficients in the waveguide divided into two output lines and interacting with side stubs are performed in the frame of a Green's function method based on the interface response theory (IRT) of continuous media.³⁶ The IRT enables to calculate also total and local densities of states. We shall avoid the details of this calculation which is given in the chapter 2 of our book.³⁷

Before giving the results of the demultiplexer based on MIT resonances, it is interesting to recall the main results about the possibility to realize MIT resonances from two detuned magnonic stub waveguides placed at the same position along the main waveguide. The cross structure is formed with two resonators of lengths d_1 and d_2 grafted on a waveguide at the same position (Fig. 2). In this structure each resonator causes the appearance of a zero of transmission. In the case where the two resonators have different lengths ($d_1 \neq d_2$), two different transmission zeros are obtained. Between the two zeros the overall resonator of length $d_0 = d_1 + d_2$ induces a transmission reaching unity giving rise to an MIT resonance shape, i.e., a resonance squeezed between two transmission zeros.

To visualize this type of resonance in a cross structure, we calculate the transmission and reflection coefficients using the inverse of the Green's function of the whole structure³⁶ at the connection point 0. The inverse of this matrix is obtained by superimposing the inverse elements of each connected guide, i.e., the two resonators and the two semi-infinite waveguides. The expressions of the inverse of the surface Green's function element of each dangling resonator (stub) i grafted vertically at a given site 0 when the boundary conditions at the ends of the stubs are vanishing magnetic current (i.e., the derivative of magnetic field) is given by $-j \frac{FC_i}{S_i}$ and the expression of the inverse of the surface element of the Green's function of each semi-infinite waveguide surrounding the two stubs is given by $-F$ where $F = jDk/\gamma M_0$, $j = \sqrt{-1}$, $S_i = \sin(kd_i)$ and $C_i = \cos(kd_i)$ with $i = 1, 2$. For the sake of simplification, we assumed that all the waveguides and stubs are made of the same material.

Now by superposing the inverse elements of the surface Green's functions of the different constituents, we obtain the inverse interface element of the Green's function of the cross structure (Fig. 2) at

the point 0

$$g^{-1}(0,0) = -2F - \frac{jFS_1}{C_1} - \frac{jFS_2}{C_2}. \quad (2)$$

The transmission amplitude through the structure is given by

$$t = \frac{2C_1 C_2}{2C_1 C_2 - jS}, \quad (3)$$

and the reflection amplitude is given by

$$r = \frac{jS}{2C_1 C_2 - jS} \quad (4)$$

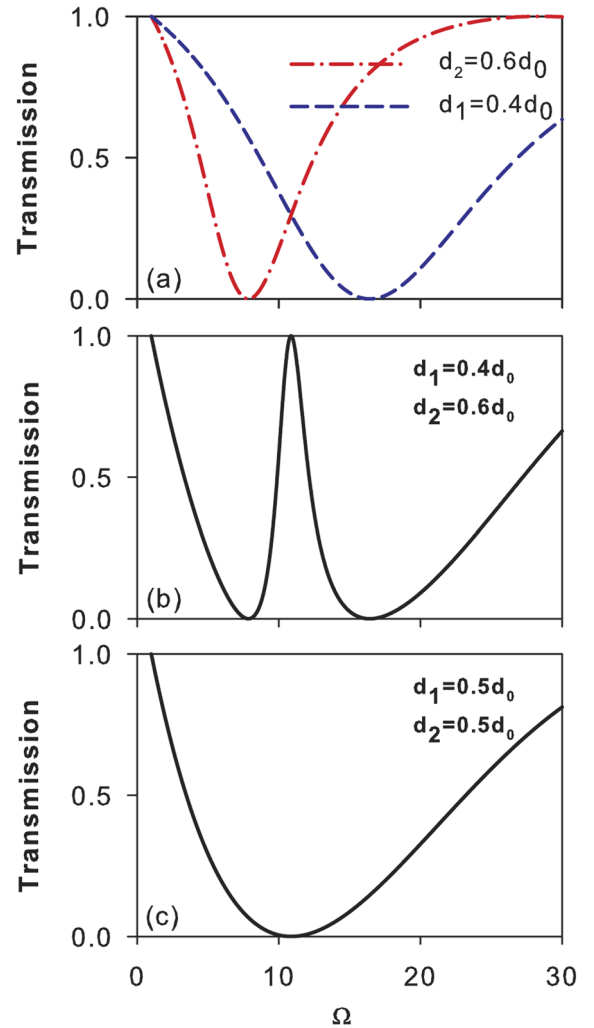


FIG. 3. Transmission as a function of the reduced frequency $\Omega = \tilde{H} + (kd_0)^2$ where $\tilde{H} = \frac{\gamma H_0 d_0^2}{D}$. (a) Case of single resonators of length $d_2 = 0.6d_0$ (dash-dot red curve) and $d_1 = 0.4d_0$ (dashed blue curve) on the waveguide. (b) Case of two resonators of lengths $d_1 = 0.4d_0$ and $d_2 = 0.6d_0$ attached at the same point on the waveguide. (c) Case of two identical resonators of lengths $d_1 = d_2 = 0.5d_0$ attached to the waveguide.

where $S = \sin(k(d_1 + d_2))$. From the expressions of the transmission and reflection coefficients $T = |t|^2$ and $R = |r|^2$, one can deduce easily the conservation energy, namely $R + T = 1$. It is well established that the connection of a single resonator along the waveguide gives rise to a transmission zero associated to the eigenmodes of the resonator with vanishing the amplitude at the bottom side connected to the waveguide, namely when $C_1 = 0$ or $C_2 = 0$. Figure 3(a) gives the transmission spectra when a single stub of length $d_1 = 0.4d_0$ (blue curve) or $d_2 = 0.6d_0$ (red curve) is attached on the side of the waveguide versus the reduced frequency $\Omega = \tilde{H} + (kd_0)^2$ where $\tilde{H} = \gamma H_0 d_0^2 / D$. One can notice the existence of transmission zeros at the reduced frequencies $\Omega_1 = 7.85$ or $\Omega_2 = 16.42$ respectively (Figs. 3(a)).

Figure 3(b) shows the transmission through the cross structure where we have connected the two resonators at the same point. The spectra shows that the position of the transmission zeros are same as before, see the comparison between the plots presented in Figs. 3(a) and 3(b). Between the two zeros (Fig. 3(b)) there exists a resonance that reaches unity, this resonance is the result of the constructive interference between the two modes of the two resonators. When the lengths of the resonators become identical (i.e., $C_1 = C_2 = 0$), then the two transmission zeros fall at the same reduced frequency $\Omega = \pi^2 + 1$, then the width of the resonance vanishes (Fig. 3(c)). This kind of zero-width resonance, characterized by an infinite quality factor, is called bound in continuum (BIC) state.³⁸ Indeed, this

mode corresponds to a confined mode in the two vertical stubs without interaction with the main horizontal guide. Therefore, this mode remains localized in the two stubs and do not radiate energy in the semi-infinite waveguides with which they are connected. In this case, instead of having a total transmission, we obtain a double transmission zero, which renders the system opaque around the reduced frequency $\Omega = \pi^2 + 1$ (Fig. 3(c)). These results clearly show that by detuning the lengths of the two resonators, we can render an opaque system transparent within a given frequency range. This is a characteristic of an MIT resonance squeezed between two transmission zeros.

In addition to the transmission and reflection coefficients, the Green's functions also allow us to calculate the density of states (DOS) which provides a supplementary information on the weight of the modes in the system. The DOS is defined from the imaginary part of the Green's function as $DOS = -1/\pi \text{Im}(g(0, 0))$ where $g(0, 0)$ is obtained from Eq. (2). In Figs. 4(a) and (b) we have presented the DOS as a function of the reduced frequency Ω in order to analyze the MIT resonance and the possibility of existence of BIC state. The results presented in Figs. 4(a) and (b) concern the DOS for the same geometries as in Figs. 3(b) and (c) respectively and clearly show the existence of a resonance around $\Omega_r = 10.86$. This resonance is similar to that obtained in Fig. 3(b); its width decreases when δ decreases and give rise to a BIC state for $\delta = 0$ (i.e., $d_1 = d_2$) as it is shown in Fig. 4(b).

III. Y-SHAPED MAGNONIC DEMULTIPLEXER BASED ON MIT RESONANCE

A. Transmission and reflection coefficients

Let us consider the structure depicted in Fig. 1. This demultiplexer consists of an input line and two output lines, all attached at the point 0. The first output line contains two stubs of lengths d_1 and d_2 inserted at the same site 1 at a distance d_5 from the entrance 0. Similarly, the second output line of the demultiplexer contains two stubs of lengths d_3 and d_4 inserted at the same site 4 at a distance d_6 from the entrance 0.

The calculation of the transmission and reflection coefficients is performed within the Green's function method. For this, we need only the inverse of the Green's function the interface space $M = \{0, 1, 4\}$, the inverse of the Green function of the whole structure (demultiplexer) described in Fig. 1 is obtained by the superposition of the inverse Green's function of its elementary constituents, namely: i) the inverse of the surface Green's function element of the three semi-infinite waveguides constituting the input and the two output lines. Their expressions are given by $[g_s(0, 0)]^{-1} = [g_s(1, 1)]^{-1} = [g_s(4, 4)]^{-1} = -F$. ii) The inverse of the surface Green's functions of the dangling resonators (stubs) grafted at the sites $\{1\}$ and $\{4\}$. Their expressions are given by $[g_i(1, 1)]^{-1} = [g_i(4, 4)]^{-1} = -F_i S_i / C_i$, where $C_i = \cosh(\alpha_i d_i)$, $S_i = \sinh(\alpha_i d_i)$ ($i = 1, 2, 3, 4$). The boundary conditions at the ends of all the stubs are those of vanishing magnetic current (i.e., the derivative of magnetic field). iii) The segments of lengths d_5 and d_6 are bounded by two surfaces located at the sites $M_1 = \{0, 1\}$ and $M_2 = \{0, 4\}$ respectively (Fig. 1). These surface elements can be written in the form of a (2×2) matrix $g_i(MM)$ within the interface space $M_1 = \{0, 1\}$ for the segment 5 and $M_2 = \{0, 4\}$ for the segment 6 (Fig. 1). The inverse of this matrix takes the following form:³⁹

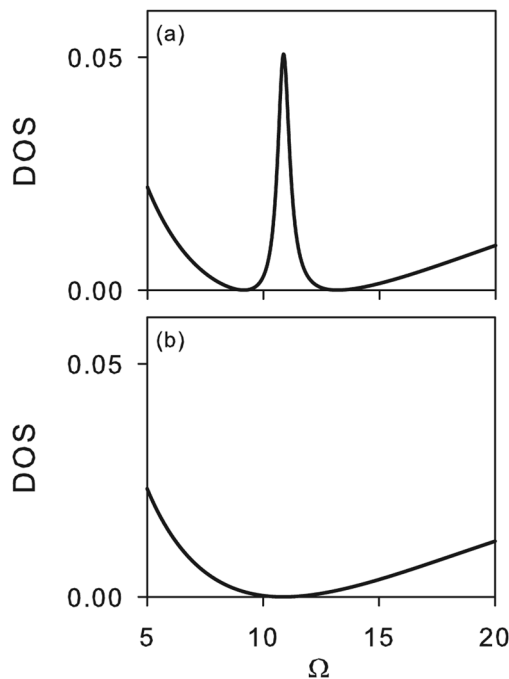


FIG. 4. Density of states (DOS) as a function of the reduced frequency $\Omega = \tilde{H} + (kd_0)^2$. (a) Case of two resonators of lengths $d_1 = 0.4d_0$ and $d_2 = 0.6d_0$ attached at the same point on the waveguide. (b) Case of two identical resonators of lengths $d_1 = d_2 = 0.5d_0$ attached to the waveguide.

$$[g_i(MM)]^{-1} = \begin{pmatrix} -\frac{F_i C_i}{S_i} & \frac{F_i}{S_i} \\ \frac{F_i}{S_i} & -\frac{F_i C_i}{S_i} \end{pmatrix}, \quad (5)$$

In what follows, we suppose that all the wires (medium) have the same characteristics (*i.e.*, $F_1 = F_2 = F_3 = F_4 = F_5 = F_6 = F$). The linear superposition of the inverse of the Green functions of the preceding constituents gives us the inverse of the Green function of the composite structure (Fig. 1) in the interface space $M = \{0, 1, 4\}$, namely

$$[g(MM)]^{-1} = -F \begin{pmatrix} \frac{C_5}{S_5} + \frac{C_6}{S_6} + 1 & -\frac{1}{S_5} & -\frac{1}{S_6} \\ -\frac{1}{S_5} & \frac{C_5}{S_5} + \frac{S_1}{C_1} + \frac{S_2}{C_2} + 1 & 0 \\ -\frac{1}{S_6} & 0 & \frac{C_6}{S_6} + \frac{S_3}{C_3} + \frac{S_4}{C_4} + 1 \end{pmatrix}. \quad (6)$$

Consider an incident spin wave $U(x) = e^{jkx}$ that comes from the left side of the semi-infinite guide (Fig. 1). The reflection amplitude wave in the input line of the demultiplexer (Fig. 1) is given by³⁹ $r = -1 - 2F_i g(0, 0)$ or equivalently

$$r = -\frac{\xi_1 + j\xi_2}{\chi_1 + j\chi_2}, \quad (7)$$

where

$$\xi_1 = C_1 C_2 C_3 C_4 (S_5 S_6 - C_5 C_6) + C_1 C_2 S' C_6 S_5 + C_3 C_4 S C_5 S_6 + S S' S_5 S_6 \quad (8)$$

$$\xi_2 = C_1 C_2 C_3 C_4 S_0 + C_1 C_2 S' C_5 C_6 + C_3 C_4 S C_5 C_6 - S_0 S S' \quad (9)$$

$$\chi_1 = 3C_1 C_2 C_3 C_4 (S_5 S_6 - C_5 C_6) + C_1 C_2 S' (S_0 + C_5 S_6) + C_3 C_4 S (S_0 + C_6 S_5) - S S' S_5 S_6 \quad (10)$$

$$\chi_2 = C_1 C_2 C_3 C_4 (3C_6 S_5 + 3C_5 S_6) + (C_5 C_6 - 2S_5 S_6) (C_1 C_2 S' + C_3 C_4 S) - S_0 S S' \quad (11)$$

and $S = \sin(k(d_1 + d_2))$, $S' = \sin(k(d_3 + d_4))$, $S_0 = \sin(k(d_5 + d_6))$.

The expression of the reflection R in the input line is given by

$$R = |r|^2. \quad (12)$$

The amplitude of the transmitted waves in the output lines 1 and 2 (Fig. 1) are given respectively by³⁹ $t_1 = -2Fg(0, 1)$ and $t_2 = -2Fg(0, 4)$, or equivalently

$$t_1 = \frac{2C_1 C_2 (-C_6 C_3 C_4 + S' S_6 + jC_3 C_4 S_6)}{\chi_1 + j\chi_2}, \quad (13)$$

$$t_2 = \frac{2C_3 C_4 (-C_5 C_1 C_2 + S S_5 + jC_1 C_2 S_5)}{\chi_1 + j\chi_2}. \quad (14)$$

The transmission coefficients in the two output lines are given respectively by

$$T_1 = |t_1|^2 \quad (15)$$

and

$$T_2 = |t_2|^2. \quad (16)$$

From Eqs. (7)–(16), one can check that the transmission and reflection coefficients satisfy the energy conservation: $T_1 + T_2 + R = 1$.

B. Demultiplexing phenomenon and Fano-shape behavior of MIT

Based on the parameters of the system, we are able to specify the necessary conditions to arrive at a total transmission on each output with a given frequency. Indeed, from Eqs. (7), (13) and (14), one can show easily that in order to realize $|T_1| = 1$, $T_2 = 0$ and $R = 0$, one should have $C_3 C_4 = 0$ (*i.e.*, $C_3 = 0$ or $C_4 = 0$), $S = 0$ and $C_6 = 0$. Similarly, in order to realize $|T_2| = 1$, $T_1 = 0$ and $R = 0$, one should have $C_1 C_2 = 0$ (*i.e.*, $C_1 = 0$ or $C_2 = 0$), $S' = 0$ and $C_5 = 0$. Now, in order to realize both conditions (*i.e.*, $|T_1| = 1$ and $|T_2| = 1$ at closed frequencies), one can show easily that the six lengths d_1 , d_2 , d_3 , d_4 , d_5 and d_6 , should satisfy the following conditions:

$$d_3 = \frac{d_1 + d_2}{2}, \quad (17)$$

$$d_4 = \frac{3d_2 - d_1}{2}, \quad (18)$$

$$d_5 = d_2, \quad (19)$$

$$d_6 = d_3. \quad (20)$$

As we have shown above (section II), in order to realize a magnonic induced resonance, one should take the lengths of the two stubs along the waveguide slightly different (*i.e.*, $\delta = d_2 - d_1 \neq 0$). Also, in this study we shall take the length of the two stubs (*i.e.*, $d_0 = d_2 + d_1$) unchanged, which fix the position of the induced resonance along the output 1. Therefore, the above conditions (Eqs. (17), (18), (19) and (20)) become respectively:

$$d_1 = \frac{d_0}{2} - \frac{\delta}{2}, \quad (21)$$

$$d_2 = d_5 = \frac{d_0}{2} + \frac{\delta}{2}, \quad (22)$$

$$d_3 = d_6 = \frac{d_0}{2}, \quad (23)$$

$$d_4 = \frac{d_0}{2} + \delta. \quad (24)$$

To visualize the previous analytical calculations, we present in Fig. 5 the variation of the transmission coefficients T_1 , T_2 and the reflection coefficient R versus the dimensionless frequency $\Omega = \tilde{H} + (kd_0)^2$ for different values of δ around $\delta = 0$. Figure 5 clearly shows that when the transmission in the first output (blue line) is unity ($T_1 = 1$), the transmission in the second output T_2 (red line) and the reflection R (black line) vanish (*i.e.*, $T_2 = R = 0$). Similarly, when the transmission in the second output (red line) is unity ($T_2 = 1$), the transmission in the first output T_1 (blue line) and the reflection R (black line) vanish (*i.e.*, $T_1 = R = 0$). As mentioned above, the induced resonance in the first output falls at the same frequency ($\Omega_r = \pi^2 + 1$) whatever of δ , its width decreases when δ decreases and vanishes for $\delta = 0$ (Fig. 3(c)). However, the shape and the width

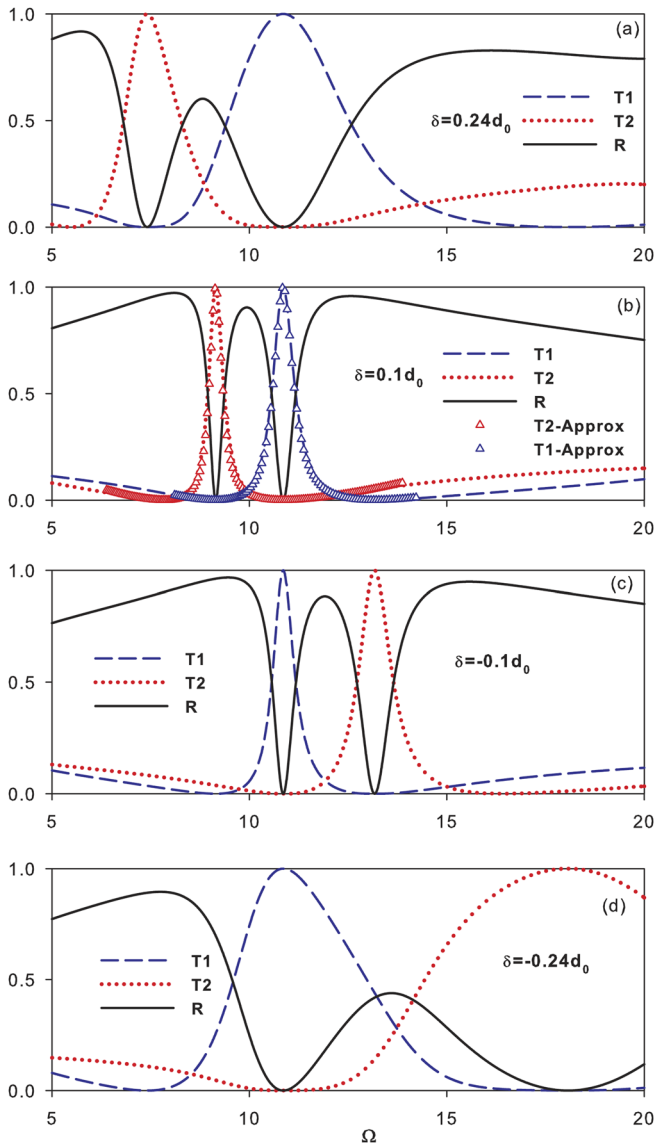


FIG. 5. Variation of the intensity of the transmitted signal in the output 1 (blue line), output 2 (red line) and the reflected signal in the input of the demultiplexer (black line) versus the dimensionless frequency $\Omega = \tilde{H} + (kd_0)^2$ for different values of $\delta = d_2 - d_1$ and for $d_0 = d_1 + d_2$ fixed.

of magnonic induced resonance slightly changes when δ becomes negative (i.e., when permuting the two stubs 1 and 2). This apparently surprising behavior results from the fact that by changing delta in the first output, we change simultaneously the value of d_4 (see Eq. (24)) in the second output. The position and the width of the resonance in the second output depend strongly on δ . Indeed, as the first magnonic induced resonance exhibits two transmission zeros around Ω_r , the position of the second resonance falls below $\Omega_r = \pi^2 + 1$ for $\delta < 0$ at the left hand side zero, crosses the first resonance at $\delta = 0$ and reappears above Ω_r for $\delta > 0$ at the right hand side

zero (Fig. 5). This is illustrated in the inset of Fig. 7 where the cross resonances occurs at $\delta = 0$.

The two filtered resonances exhibit an induced transparency-like shape, i.e. a resonance squeezed between two transmission zeros induced by the stubs falling at the same frequency where the system has been opaque. Indeed, a Taylor expansion of the transmission amplitude (Eq. (13)) around the resonance at Ω_r (i.e., $\Omega = \Omega_r + \epsilon$), enables us to write T_1 following the induced transparency-like resonance, namely

$$T_1 = A \frac{(\epsilon + q_1\Gamma)^2(\epsilon + q_2\Gamma)^2}{\epsilon(\epsilon + \beta) + \Gamma^2}, \quad (25)$$

where $A = \frac{(\frac{1}{4} - \frac{\Delta^2}{\pi^2})^2}{\frac{1}{4} + \frac{5\Delta^2}{8} + \frac{\Delta^3}{2\pi^2}}$, $\beta = \frac{(\frac{4\Delta^4}{\pi} - \Delta^5 + \frac{6\Delta^6}{\pi})}{\frac{1}{4} + \frac{5\Delta^2}{8} + \frac{\Delta^3}{2\pi^2}}$ and $\Delta = -\pi\delta/2d$.

The full width at half maximum of the induced resonance falling at $\epsilon = 0$ (i.e., Ω_r) is given by

$$\Gamma = \frac{\Delta^2}{(\frac{1}{4} + \frac{5\Delta^2}{8} + \frac{\Delta^3}{2\pi^2})^{1/2}}, \quad (26)$$

$q_1 = \frac{\Delta}{\Gamma(\frac{1}{2} + \frac{\Delta}{\pi})}$ and $q_2 = -\frac{\Delta}{\Gamma(\frac{1}{2} - \frac{\Delta}{\pi})}$ are the Fano parameters.

They give qualitatively the strength of the interference between the bound state and the propagating continuum states.^{40,41} One can notice that when increasing δ from 0, Γ increases (i.e., the quality factor decreases) and q decreases. The approximate expression for the second transmission coefficient T_2 can be obtained by following the same procedure where we consider $d_0 = d_3 + d_4$ instead of $d_1 + d_2$. However, from Eqs. (17)–(20), $d_4 - d_3$ keep the same value as $d_2 - d_1$. An example of the results of the approximate expression (Eq. (25)) is shown by the red triangles in Fig. 5(b) for $\delta = 0.1$ and clearly shows that the resonance is induced transparency-like with $q_1 = -7.4$, $q_2 = 6.06$ and width $2\Gamma = 0.03\pi$. In addition, in the periodic systems, a perturbation is often introduced to the system in order to create the resonance state in the gap.⁴² However, the above calculation shows that, without introducing any perturbation in the structure, one can find a well defined a MIT resonance with a width 2Γ and coupling parameters q_1 and q_2 that can be adjusted by tailoring the lengths of the resonators (i.e. δ).

Figure 6 shows an analysis of the DOS at the connecting points 0, 1 and 4 of the demultiplexer (Fig. 1): 0 (black curve), 1 (blue

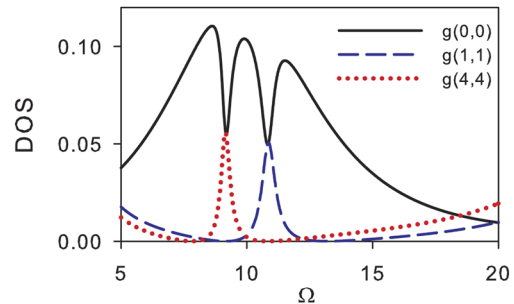


FIG. 6. Density of states (DOS) as a function of the reduced frequency at the connecting points 0, 1 and 4 of the demultiplexer (Fig. 1): 0 (black curve), 1 (blue curve), and 4 (red curve) for $\delta = 0.1d_0$.

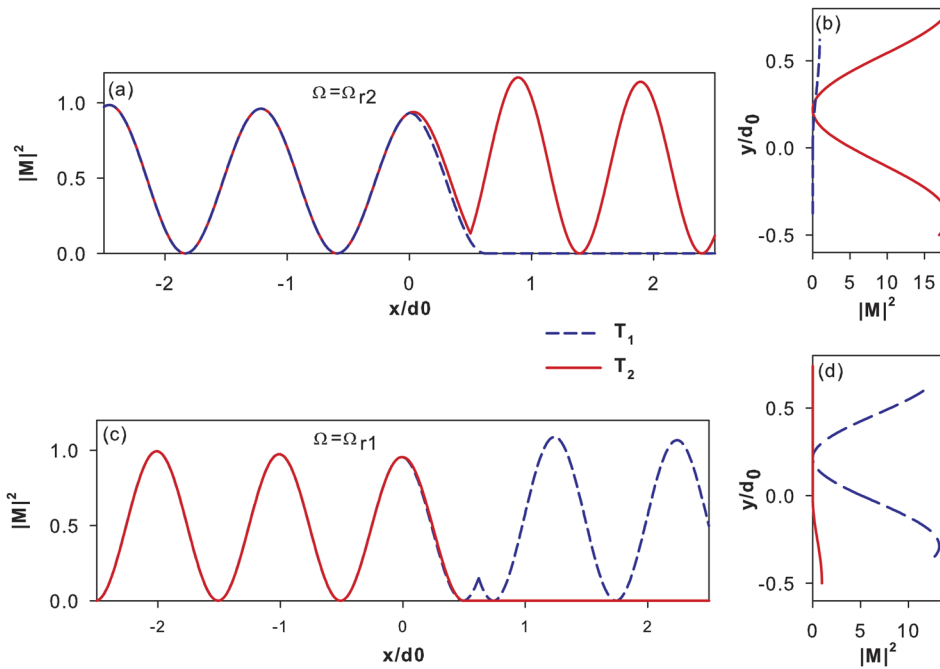


FIG. 7. Square modulus of the magnetization field $|M|^2$ versus the space position of the system. The blue (red) curves represent the intensity of the field in the first (second) line. (a) and (c) give the behavior of $|M|^2$ along the horizontal lines whereas (b) and (d) show the behavior of $|M|^2$ along the vertical stubs in each line. These fields are plotted for the dimensionless frequency $\Omega_{r2} = 7.38$ ((a) and (b)) and $\Omega_{r1} = 10.86$ ((c) and (d)).

curve), and 4 (red curve). These results are plotted for the same parameters as in Fig. 5(b), namely $\delta = 0.1d_0$. One can notice that the DOS at the exit points 1 and 4 exhibit similar behaviors as the transmission coefficients T_1 and T_2 in Fig. 5(b), that is the DOS presents a maximum on one line at the same frequency where it vanishes on the other line and vice-versa. However, the DOS at the input point 0 shows dips at both resonances without reaching zeros as for the reflection (black curve in Fig. 5(b)). This is due to the fact the reflection coefficient is not proportional to the term $g(0, 0)$ as it is the case for the DOS.

In order to analyze the spatial confinement^{43,44} of the different modes filtered and stopped by the demultiplexer, we have calculated the field magnetization in each part of the structure using the following expression:³⁷

$$M(x) = \frac{-2F}{S_m} \{g(0, i) \sin[k(d_m - x)] + g(0, j) \sin[k(x)]\}, \quad (27)$$

in each finite waveguide m ($m = 1-6$) delimited by the interfaces i and j ($i, j = 0-6$, see Fig. 1) and $0 \leq x \leq d_m$. The Green's function elements $g(0, i)$ and $g(0, j)$ that relates the entrance of the system and the two surfaces of each finite guide, are obtained by inverting the 7×7 matrix given in the Appendix. In the semi-infinite waveguides, the expressions of $M(x)$ are given by

$$M(x) = -2Fg(0, 0)e^{-jkx} \text{ for } x \leq 0 \text{ in the input line,} \quad (28)$$

$$M(x) = -2Fg(0, 1)e^{jk(x-d_5)} \text{ for } x \geq d_5 \text{ in the first output line,} \quad (29)$$

$$M(x) = -2Fg(0, 4)e^{jk(x-d_6)} \text{ for } x \geq d_6 \text{ in the second output line.} \quad (30)$$

Figure 7 gives the square modulus of the magnetization field for the two resonances labeled $\Omega_{r1} = 10.86$ and $\Omega_{r2} = 7.38$ for $\delta = 0.24d_0$ (Fig. 5(a)). These modes correspond respectively to a filtered resonance in one line and a stopped resonance in the other line (blue dashed and red dotted curves in Fig. 5(a)). Figures 7(a) clearly show that mode $\Omega_{r2} = 7.38$ is transferred along the second line (red curve), whereas it is stopped along the first line (dashed blue curve). The transfer of this mode along the second line is due to the excitation of both stubs of lengths d_3 and d_4 along this line as it illustrated in Fig. 7(b) (red curve), whereas its stopping along

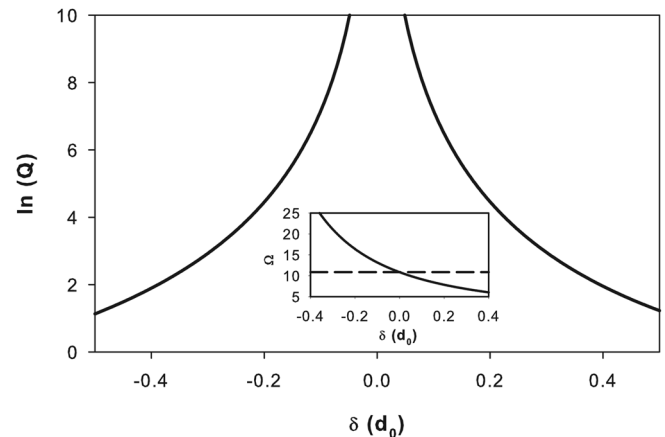


FIG. 8. The variation of the logarithm of the quality factor Q versus δ . The inset shows the variation of the positions of the two resonances in Fig. 5 as a function of δ .

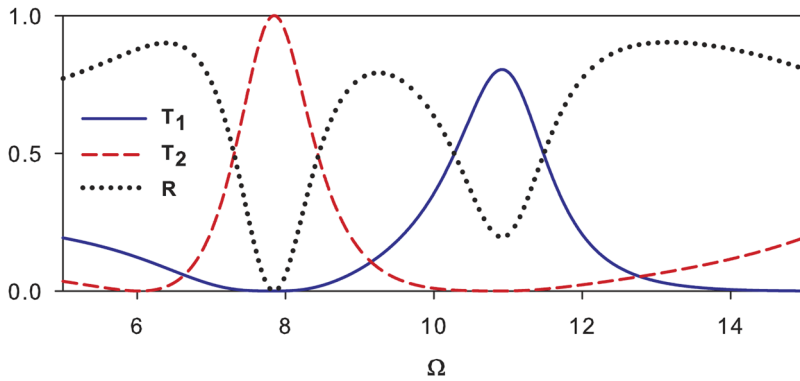


FIG. 9. The same as in Figure 5(a), except that $d_6 = 0.75d_0 \neq d_3$.

the first line is due to the excitation of the stationary mode of only the stub of length $d_2 = 0.62d_0$ as shown in Fig. 7(b) (blue dashed curve). Figures 7(c) and (d) give the same results as in Figs. 7(a) and (b) but for the MIT resonance $\Omega_{r1} = 10.86$. Here, we obtain a different behavior where the transfer occurs along the first line (blue dashed curve in Fig. 7(c)) through the excitation of its double stubs of lengths d_1 and d_2 (blue dashed curve in Fig. 7(d)), whereas the wave is stopped along the second line (red curve in Fig. 7(c)) as a consequence of the excitation of the mode of one of its stubs of length $d_3 = 0.5d_0$ (red curve in Fig. 7(d)). These results clearly show how the lengths of the finite guides constituting the demultiplexer should be engineered in order to realize a perfect demultiplexing.

Another interesting quantity that characterizes the resonances filtered along each line is the quality factor which is defined by $Q = \Omega_r/2\Gamma$, where Γ is given by Eq. (26) and Ω_r is the resonance frequency. The width of the resonances depends strongly on the difference between the lengths of the stubs (i.e., $\delta = d_2 - d_1 = d_4 - d_3$). This is illustrated in Fig. 8 where we have plotted the quality factor Q of the resonance at Ω_r . One can notice that the quality factor of the resonance depends slightly on the sign of δ and as predicted diverges when δ vanishes.

Equations (17)–(20) are necessary to be satisfied for a perfect demultiplexing (i.e., total transmission along each line). However, if one of the above conditions is not satisfied, then the transmission can not reach unity and the demultiplexing becomes imperfect. An example elucidating this deviation from perfect demultiplexing is given in Fig. 9 where we have chosen the same parameters as in Fig. 5(a) except that $d_6 = 0.75d_0 \neq d_3$. One can notice that the transmission in the first output (blue line) does not reach unity at $\Omega = 11.12$, and at the same time the reflection coefficient (black dotted line) does not reach zero. However, the deviation from perfect demultiplexing remains weak as far as the lengths of the different waveguides do not exceed 10% of the exact values. Also the transmission in one arm can be affected by the geometry of the other line. Indeed, Eqs. (17) and (18) clearly show how the lengths of the stubs d_3 and d_4 in the second line should be chosen as function of those d_1 and d_2 in the first line in order to realize perfect demultiplexing, otherwise we obtain (not shown here) a deviation from a perfect demultiplexing.

Another interesting physical quantity that can affect considerably the quality of the demultiplexer in filtering the MIT resonances, is the damping. The magnetic damping has been probed by

measuring the resonance linewidth in the frequency domain using the ferromagnetic resonance (FMR) technique⁴⁵ that makes accurate predictions about the magnetization dynamics. Two mechanisms are behind the linewidth FMR, one intrinsic which is related to spin-orbit coupling and magnon-phonon scattering and the other extrinsic which is due to the presence of inhomogeneities or imperfections within the crystal. In a ferromagnetic system, the spin dynamics is described by using Landau-Lifshitz-Gilbert (LLG) equation in which a phenomenological dimensionless parameter α defines a magnetization relaxation.⁴⁶ In order to take into account this effect, we have introduced a phenomenological damping factor Γ and therefore the wave-vector k in Eqs. (7), (13) and (14) becomes complex: $k = k_R + jk_I$ where $k_R = \sqrt{\frac{\omega - \gamma H_0}{D}}$ and $k_I = \frac{\Gamma}{2\sqrt{D(\omega - \gamma H_0)}}$ are real and imaginary parts of the wave-vector in the different waveguides. The LLG parameter α is related to Γ by the equation $\alpha = \frac{\Gamma}{\gamma H_0}$.

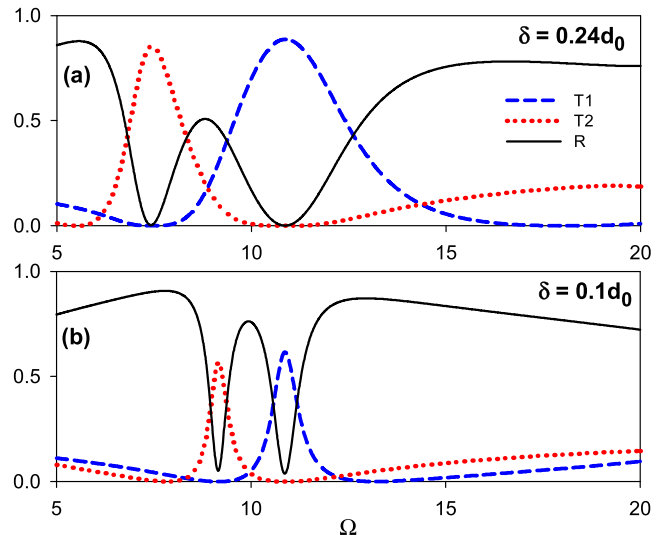


FIG. 10. Transmission spectra in the output 1 (dashed blue line), output 2 (dotted red line) and the reflected wave in the input of the demultiplexer (black line) versus the dimensionless frequency $\Omega = \bar{H} + (kd_0)^2$ for $\delta = 0.24d_0$ (a) and $\delta = 0.1d_0$ (b). These figures are similar to Figs. 5(a) and (b) respectively but in presence of loss in the waveguides.

Figures 10(a) and (b) give the same results as in Figs. 5(a) and (b) but in presence of damping. We suppose that waveguides are made of Permalloy (Py) material characterized by the parameter $\alpha = 0.008$. Py is the most common material used in magnonics research, it offers low damping and isotropic magnetic properties.^{1,47,48} We can notice that the transmission spectra in Fig. 10(a) (blue and red curves) exhibit the same behavior as in Fig. 5(a), however, as predicted the resonances do not reach unity because of the attenuation in the waveguides. Also, the reflection spectra (black curve) is less affected. However, when δ decreases the effect of damping on the intensity of thin MIT resonances (Fig. 5(b)) becomes important as it is shown in Fig. 10(b) for $\delta = 0.1d_0$, also the reflection does not reach zero at the positions of both MIT resonances (black curve in Fig. 10(b)).

IV. CONCLUSION

In this paper we have shown theoretically the possibility to realize a simple magnonic demultiplexer based on magnonic induced transparency resonances. The demultiplexer design has the form of Y-shaped waveguide with one input line and two output lines. Each line contains two grafted stubs at a given position far from the input line. We derived closed form expressions for the waveguide lengths to achieve selective transfer of a single propagating mode through one line keeping the other line unaffected. The position and the width of the resonances depend on the different lengths of the waveguides which should be chosen appropriately. Also, we have shown that the transmission can be written following the Fano-like form, which enables us to deduce the position, the width (or the quality factor) and the Fano parameters of the resonances as a function of the detuning parameter δ between the two stubs in the first line. In addition to the transmission and reflection study, we have given an analysis of the density of states of the different

modes in the system. The confinement of the filtered and stopped resonances along each line are demonstrated through an analysis of the magnetization field. The effect of loss on the quality of the demultiplexer in filtering and stopping different frequencies is also discussed.

The demultiplexer proposed in this study presents several advantages in comparison with those based on magnonic crystals such as: i) the simplicity of the device from the technological point of view, where we need only two resonators on each output line instead of a periodic structure with a given defect, ii) the simplicity of the structure renders the calculation analytical which enables to deduce the exact expressions of the different lengths of the waveguides to realize a perfect demultiplexing. iii) The possibility to increase the quality factor of the filtered resonances close to infinity by detuning the two stubs. This property is a characteristic of induced transparency resonances and does not exist in standard one-dimensional magnonic crystals with defects where filtering occurs through Breit-Wigner resonances with finite width. Finally, let us mention that the results presented in this paper can be transposed straightforwardly to acoustic demultiplexers based on waveguide tubes.^{27,49,50}

APPENDIX: THE WHOLE INTERFACE GREEN'S FUNCTION OF THE DEMULTIPLEXER

In order to calculate the magnetization field associated to different modes in the demultiplexer structure (Fig. 1), we need the inverse of the Green's function of the whole system in the space of interface composed of seven interfaces, namely $M = \{0, 1, 2, 3, 4, 5, 6\}$. From the expressions of the inverse Green's function of each piece (Eq. (5)), one can construct the inverse Green's function $g^{-1}(MM)$ of the whole system as follows (the details of this calculation are given in the chapter 2 of our book³⁷).

$$[g(MM)]^{-1} = -F \begin{pmatrix} \frac{C_5}{S_5} + \frac{C_6}{S_6} + 1 & \frac{-1}{S_5} & 0 & 0 & \frac{-1}{S_6} & 0 & 0 \\ \frac{-1}{S_5} & \frac{C_5}{S_5} + \frac{C_1}{S_1} + \frac{C_2}{S_2} + 1 & \frac{-1}{S_1} & \frac{-1}{S_2} & 0 & 0 & 0 \\ 0 & \frac{-1}{S_1} & \frac{C_1}{S_1} & 0 & 0 & 0 & 0 \\ 0 & \frac{-1}{S_2} & 0 & \frac{C_2}{S_2} & 0 & 0 & 0 \\ \frac{-1}{S_6} & 0 & 0 & 0 & \frac{C_6}{S_6} + \frac{C_3}{S_3} + \frac{C_4}{S_4} + 1 & \frac{-1}{S_3} & \frac{-1}{S_4} \\ 0 & 0 & 0 & 0 & \frac{-1}{S_3} & \frac{C_3}{S_3} & 0 \\ 0 & 0 & 0 & 0 & \frac{-1}{S_4} & 0 & \frac{C_4}{S_4} \end{pmatrix}. \quad (A1)$$

After inverting this matrix numerically, we get the different Green's functions elements between the interface 0 and any interface i ($i = 0 - 6$) (Fig. 1); these elements are needed for the calculation of the magnetization at different position in the system (Eqs. (27)–(30)).

REFERENCES

- 1 A. V. Chumak, A. A. Serga, and B. Hillebrands, *J. Phys. D: Appl. Phys.* **50**, 244001 (2017).
- 2 A. V. Sadovnikov, E. N. Beginin, K. V. Bublikov, S. V. Grishin, S. E. Sheshukova, Yu. P. Sharaevskii, and S. A. Nikitov, *J. Appl. Phys.* **118**, 203906 (2015).

- ³M. M. Eshaghian-Wilner, A. Khitun, S. Navab, and K. L. Wang, *Spin-wave architectures Bio-inspired and Nanoscale Integrated Computing*, ed M. M. Eshaghian-Wilner (Hoboken, NJ, Wiley) 2009.
- ⁴A. V. Chumak, V. I. Vasyuchka, A. A. Serga, and B. Hillebrands, *Nat. Phys.* **11**, 453 (2015).
- ⁵V. V. Kruglyak, S. O. Demokritov, and D. Grundler, *J. Phys. D: Appl. Phys.* **43**, 264001 (2010).
- ⁶M. Mruczkiewicz, M. Krawczyk, V. K. Sakharov, Yu. V. Khivintsev, Yu. A. Filimonov, and S. A. Nikitov, *J. Appl. Phys.* **113**, 093908 (2013).
- ⁷K. Vogt, F. Y. Fradin, J. E. Pearson, T. Sebastian, S. D. Bader, B. Hillebrands, A. Hoffmann, and H. Schultheiss, *Nat. Commun.* **5**, 3727 (2014).
- ⁸V. E. Demidov, S. Urazhdin, A. Zholud, A. V. Sadovnikov, A. N. Slavin, and S. O. Demokritov, *Sci. Rep.* **5**, 8578 (2015).
- ⁹D. Grundler, *Nat. Phys.* **11**, 438 (2015).
- ¹⁰Yu. S. Dadoenkova, N. N. Dadoenkova, I. L. Lyubchanskii, J. W. Klos, and M. Krawczyk, *J. Appl. Phys.* **120**, 073903 (2016).
- ¹¹S. Tacchi, G. Gubbiotti, M. Madami, and G. Carlotti, *J. Phys.: Condens. Matter* **29**, 073001 (2017).
- ¹²M. P. Kostylev, A. A. Serga, T. Schneider, B. Leven, and B. Hillebrands, *Appl. Phys. Lett.* **87**, 153501 (2005).
- ¹³A. Khitun and K. L. Wang, *Superlattices Microstruct.* **38**, 184 (2005).
- ¹⁴H. Takagi, J. Noda, T. Ueno, N. Kanazawa, Y. Nakamura, and M. Inoue, *Electron. Commun. Japan* **97**, 833 (2014).
- ¹⁵A. V. Sadovnikov, S. A. Odintsov, E. N. Beginin, S. E. Sheshukova, Yu. P. Sharaevskii, and S. A. Nikitov, *Phys. Rev. B* **96**, 144428 (2017).
- ¹⁶A. V. Sadovnikov, A. A. Grachev, S. E. Sheshukova, Yu. P. Sharaevskii, A. A. Serdobintsev, D. M. Mitin, and S. A. Nikitov, *Phys. Rev. Lett.* **120**, 257203 (2018).
- ¹⁷A. V. Sadovnikov, A. A. Grachev, V. A. Gubanov, S. A. Odintsov, A. A. Martyshkin, S. E. Sheshukova, Yu. P. Sharaevskii, and S. A. Nikitov, *Appl. Phys. Lett.* **112**, 142402 (2018).
- ¹⁸A. V. Sadovnikov, A. A. Grachev, E. N. Beginin, S. E. Sheshukova, Yu. P. Sharaevskii, and S. A. Nikitov, *Phys. Rev. Applied* **7**, 014013 (2017).
- ¹⁹A. V. Sadovnikov, E. N. Beginin, M. A. Morozova, Yu. P. Sharaevskii, S. V. Grishin, S. E. Sheshukova, and S. A. Nikitov, *Appl. Phys. Lett.* **109**, 042407 (2016).
- ²⁰A. V. Sadovnikov, V. A. Gubanov, S. E. Sheshukova, Yu. P. Sharaevskii, and S. A. Nikitov, *Phys. Rev. Applied* **9**, 051002 (2018).
- ²¹A. V. Chumak, A. A. Serga, S. Wolff, B. Hillebrands, and M. P. Kostylev, *Appl. Phys. Lett.* **94**, 172511 (2009).
- ²²Y. Zhu, K. H. Chi, and C. S. Tsai, *Appl. Phys. Lett.* **105**, 022411 (2014).
- ²³A. V. Chumak, A. A. Serga, and B. Hillebrands, *Nat. Commun.* **5**, 4700 (2014).
- ²⁴M. D. Eisaman, A. Andre, F. Massou, M. Fleischhauer, A. S. Zibrov, and M. D. Lukin, *Nature* **438**, 837 (2005).
- ²⁵M. F. Yanik and S. Fan, *Phys. Rev. Lett.* **92**, 083901 (2004).
- ²⁶Q. Xu, S. Sandhu, M. L. Povinelli, J. Shakya, S. Fan, and M. Lipson, *Phys. Rev. Lett.* **96**, 123901 (2006).
- ²⁷A. Merkel, G. Theocharis, O. Richoux, V. Romero-Garcia, and V. Pagneux, *Appl. Phys. Lett.* **107**, 244102 (2015).
- ²⁸A. Mouadili, E. H. El Boudouti, A. Soltani, A. Talbi, A. Akjouj, and B. Djafari-Rouhani, *J. Appl. Phys.* **113**, 164101 (2013).
- ²⁹A. Mouadili, E. H. El Boudouti, A. Soltani, A. Talbi, B. Djafari-Rouhani, A. Akjouj, and K. Haddadi, *J. Phys.: Condens. Matter* **26**, 505901 (2014).
- ³⁰A. Mouadili, E. H. El Boudouti, H. Al-Wahsh, A. Akjouj, B. Djafari-Rouhani, and L. Dobrzynski, IEEE 2017 International Conference on Electrical and Information Technologies (ICEIT), Rabat, Morocco.
- ³¹Z. J. Tay, W. T. Soh, and C. K. Ong, *J. Magn. Magn. Mater.* **451**, 235 (2018).
- ³²C. J. Dai, X. H. Yan, Y. Xiao, and Y. D. Guo, *J. Magn. Magn. Mater.* **379**, 167 (2015).
- ³³M. G. Cottam and D. R. Tilley, *Introduction to surface and superlattice excitations* (Cambridge University Press, 1989).
- ³⁴K. H. Bennemann and J. B. Ketterson, *Novel superfluids*, Volume 2, Oxford University Press (2014).
- ³⁵E. L. Albuquerque and M. G. Cottam, *Physics Reports* **376**, 225337 (2003) and references therein.
- ³⁶H. Al-Wahsh, A. Akjouj, B. Djafari-Rouhani, and L. Dobrzynski, *Surf. Sci. Rep.* **66**, 29 (2011).
- ³⁷A. Akjouj, L. Dobrzynski, H. Al-Wahsh, E. H. El Boudouti, G. Levêcque, Y. Pennec, and B. Djafari-Rouhani, Chapter 2 (p. 53), *Magnonics*, Elsevier (2019).
- ³⁸C. W. Hsu, B. Zhen, A. D. Stone, J. D. Joannopoulos, and M. Soljačić, *Nat. Rev. Mater.* **1**, 16048 (2016).
- ³⁹H. Al-Wahsh, E. H. El Boudouti, B. Djafari-Rouhani, A. Akjouj, T. Mrabti, and L. Dobrzynski, *Phys. Rev. B* **78**, 075401 (2008).
- ⁴⁰C. H. Raymond Ooi and C. H. Kam, *Phys. Rev. B* **81**, 195119 (2010).
- ⁴¹B.-B. Li, Y.-F. Xiao, C.-L. Zou, X.-F. Jiang, Y.-C. Liu, F.-W. Sun, Y. Li, and Q. Gong, *Appl. Phys. Lett.* **100**, 021108 (2012).
- ⁴²E. H. El Boudouti, N. Fettouhi, A. Akjouj, B. Djafari-Rouhani, A. Mir, J. O. Vasseur, L. Dobrzynski, and J. Zemmouri, *J. Appl. Phys.* **95**, 1102 (2004).
- ⁴³V. E. Demidov, S. Urazhdin, A. Zholud, A. V. Sadovnikov, and S. O. Demokritov, *Appl. Phys. Lett.* **106**, 022403 (2015).
- ⁴⁴S. O. Demokritov, *Spin Wave Confinement* (Pan Stanford Publishing Pte. Ltd., 2009).
- ⁴⁵C. Kittel, *Phys. Rev.* **73**, 155 (1948).
- ⁴⁶A. Barman and J. Sinha, *Spin Dynamics and Damping in Ferromagnetic Thin Films and Nanostructures* (Springer Nature, 2018).
- ⁴⁷D. J. Twisselmann and R. D. McMichael, *J. Appl. Phys.* **93**, 6903 (2003).
- ⁴⁸S. S. Kalarickal, P. Krivosik, M. Wu, and C. E. Patton, *J. Appl. Phys.* **99**, 093909 (2006).
- ⁴⁹A. Santillan and S. I. Bozhevolnyi, *Phys. Rev. B* **84**, 064304 (2011).
- ⁵⁰E. H. El Boudouti, T. Mrabti, H. Al-Wahsh, B. Djafari-Rouhani, A. Akjouj, and L. Dobrzynski, *J. Phys.: Condens. Matter* **20**, 255212 (2008).